Materials & Design 223 (2022) 111164

Contents lists available at ScienceDirect

Materials & Design

journal homepage: www.elsevier.com/locate/matdes

Modified digital image correlation aided measurement of the transverse to longitudinal deformation ratio for polymeric macro-fibres

T. Ikumi [a,b], P. Pujadas [b,c,*], J. de la Cruz [d], I. Segura [d], A. de la Fuente [d]

[a] Smart Engineering Ltd, C/Jordi Girona, 1-3, Parc UPC – K2M, Barcelona 08034, Spain
[b] Department of Project and Construction Engineering, Polytechnic University of Catalonia (UPC), Av. Diagonal 647, Barcelona, 08028, Spain
[c] Group of Construction Research and Innovation (GRIC), C/ Colom, 11, Ed. TR5, Terrassa, Barcelona 08222, Spain
[d] Department of Civil and Environmental Engineering, Polytechnic University of Catalonia (UPC), C/ Jordi Girona 1-3, Barcelona, 08034, Spain

HIGHLIGHTS

- The novel measurement procedure presented is a cost-effective alternative for measuring the transverse-to-longitudinal deformation ratio of polymeric macro-fibres.
- The low cost of the equipment and simplicity of the procedure allows its implementation in large-scale fibre design optimization processes.
- This study reports the first transverse-to-longitudinal deformation ratios of polymeric macro-fibres commonly used in structural concrete.
- The transversal deformation is variable and non-uniform along the length for embossed fibres subjected to tension.

GRAPHICAL ABSTRACT

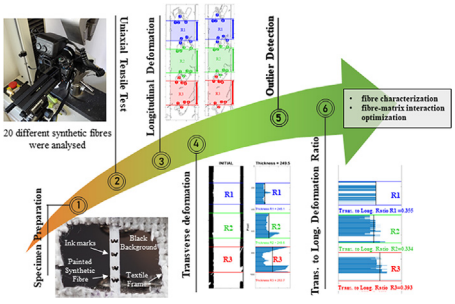

ARTICLE INFO

Article history:
Received 30 March 2022
Revised 13 September 2022
Accepted 15 September 2022
Available online 16 September 2022

Keywords:
Poisson's ratio
Polymeric macro-fibre
Concrete
Fibre reinforced concrete
DIC
Deformation

ABSTRACT

Considering the increasing interest of polymeric macro-fibres reinforced concrete, a simple and straightforward method to assess the fibre's transverse to longitudinal deformation ratio (η_f) becomes a determining aspect in terms of fibre both characterization and fibre–matrix interaction optimization. A noncontact optical measurement procedure to assess this ratio (η_f) - for concrete reinforcement - by a modified 2D Digital Image Correlation method is presented in this paper. This ratio (η_f) has influence on the matrix-fibre interaction and, thus, on the post-cracking tensile response of the concrete composite. Details on the definition, implementation and validation of this measurement procedure are presented. Additionally, an experimental program on 20 selected lab grade and commercial fibres was carried out to analyse the consistency of the measurements and the influence of the fibre's geometric characteristics (flat, curved, embossed or crimped) on the η_f. The outcomes of this research and the experimental procedure proposed are meant to assist fibre producers on the design process of optimized fibres to be used in structural concrete.

* Corresponding author at: Department of Project and Construction Engineering, School of Industrial Engineering of Barcelona (ETSEIB), Technical University of Catalonia-BarcelonaTech, Av. Diagonal 647, 08028 Barcelona, Spain.
E-mail address: pablo.pujadas@upc.edu (P. Pujadas).

https://doi.org/10.1016/j.matdes.2022.111164
0264-1275/

1. Introduction

When fibre-like materials are stretched in the longitudinal direction, the lateral directions contract to decrease the stretch-induced volume change. The ratio of lateral strain (ε_t) to applied tensile strain (ε_l) is called Poisson's ratio (ν), which is one of the parameters that govern the matrix-fibre interaction (i.e., in cement-based matrices). Fibre Poisson's ratio (ν_f) is a design parameter of materials that need to be considered when the fibre-reinforced matrix is subjected to dimensional changes resulting from the application of a force -or an imposed deformation. Likewise, for the application of the generalized theory of elasticity to structural analysis, ν_f is also an input parameter (ASTM D638-14 [1]).

In the case of polymeric macro-fibres reinforced concrete (PMFRC), some researchers have quantified -from an analytical perspective- the influence of Poisson's ratio on the pull-out mechanism of polypropylene or another polyolefin fibres oriented to reinforced cement-based composites [2–4]. In this context, for fibre reinforced composites subjected to tensile forces, both the fibre -generally with a higher Poisson ratio than that of the matrix- and matrix tend to deform differently [5]. This causes local Poisson contraction and, eventually, the level of shear force developed at the interface exceeds the total static interfacial shear strength [6], this resulting in interfacial premature and unstable debonding of the fibre from the matrix at the crack plane [4,7]. These phenomena are more evident and significant for the mechanical performance in cracked sections since in uncracked cement-based composites the contribution of fibres into the resistant mechanism is negligible. Likewise, it must be emphasized that pull-out response of a single fibre not necessarily represents the post-cracking performance of the PMFRC, which is governed by the stochastic nature of the variables involved (i.e., fibre geometry, fibre–matrix bond strength, fibre orientation, fibre embedded length, and others) in the resistant mechanism.

Consequently, the Poisson effect might have a detrimental impact of the post-cracking bearing capacity of the structure and thus, measures to reduce this are of outmost importance from both economic and structural safety reasons. In this regard, the design of polymeric macro-fibres (PMFs hereinafter) for concrete reinforcement based on optimizing the fibre Poisson's ratio is a line still unexplored. Advances in this line could be relevant in structural applications of PMFRC such as pavements [8], precast tunnels linings [9], slabs for buildings [10–12], sewerage pipes [13–16], and design-for-fatigue concrete components [17]. Improvements in these PMFRC applications can lead to significant increases of sustainability performance in several structural reinforced concrete typologies [18–24]. However, any potential use of ν_f during PMFs design and manufacturing first requires suitable method for characterizing this property.

To characterize the Poisson's ratio of materials, a uniaxial tensile load is applied and the transverse and axial deformations derived from the test are used to compute the Poisson's ratio. There are several standardized tests that can be used to determine Poisson's ratio of polymeric materials. The most common and reliable test configuration to determine this ratio is the direct measurement using a strain measuring device on a suitable specimen that complies with certain geometries and surface conditions (ASTM D638-14 [1] and ISO 527 [25]). The use of bonded strain gages is an accurate technique, but this can be costly and time consuming. Bonded strain gages are commonly used for composite materials made of high modulus fibres (i.e., carbon fibres) bound in some type of thermoset resin system. For thermoplastic materials (i.e., polypropylene or other polyolefin-based fibres), the use of biaxial contact extensometers is the most common approach.

Even though, the use of standardized specimens and testing conditions allow the characterization of the material Poisson's ratio, this property might not necessarily reflect the behaviour of PMFs used in concrete applications. Commercial PMFs differ from specimens used for Poisson's ratio determination on the production process. Macrosynthetic embossed and crimped fibres -which are the most used for concrete reinforcement- are subjected to drawing, stretching, orientation and other processes that might induce anisotropy of the resulting fibre and alter the Poisson's ratio of the virgin material. Therefore, the concept of Poisson's ratio of the material is no longer valid for these fibres and it is necessary to evaluate this property directly on the fibre as a transverse to longitudinal deformation ratio (η_f). This ratio allows recognizing the performance of the product (the fibre), including the material characteristics (Poisson's ratio).

However, contact-based measurement techniques are challenging to implement to fibre-like materials as the small cross-section of the fibre compromises the experimental assessment of such property. In this case, contact measurement techniques such as clip on or contact extensometers can lead to unreliable results due to the weight of the device and other motions triggered by the contact [26,27].

Nowadays, there are non-contacting strain measurement techniques based on video and laser extensometers that can provide additional information and productivity advantages over contact-extensometers without compromising the precision. Initially, video and laser extensometers were used only when specimens were fragile or when the energy released during fracture could damage the extensometer. Currently, optical measurement techniques such as Moiré interferometry, electronic speckle pattern interferometry and digital image correlation (DIC) are widely adopted to obtain non-contact measurements for a wide range of applications. However, most of these techniques cannot be directly applied to PMFs as certain requirements regarding specimen geometry are not attained. Moreover, the cost of laser technology based techniques can be significant and not meant for a fibre optimization processes, which could require a large number of measurements. To the author's knowledge, no studies have been conducted on the characterization of the η_f in real PMFs used in practice.

In this regard, considering the increasing interest of PMFRCs for the structural application abovementioned and the inclusion of PMFs in design guidelines of concrete structures, simple and straightforward method to assess the fibre's transverse to longitudinal deformation ratio (η_f) becomes a critical aspect in terms of fibre characterization and fibre–matrix interaction optimization. Even though this ratio might not necessarily coincide with the material Poisson's ratio (ν_f), the former could be a more representative indicator of the behaviour of the matrix-fibre interface during tensile loading and serve for comparison purposes between different (geometries and/or material compositions) PMFs.

In this context, this manuscript is aimed at describing the definition, implementation and validation phases of a novel non-contact DIC-based optical measurement procedure oriented to assess η_f of PMFs. To this purpose, an extensive experimental program focused on characterizing a number of selected polymeric macro-fibres (including lab grade and commercially available) was carried out. Finally, the consistency of the measurements and the influence of the fibre's material and geometric properties on η_f are discussed.

2. Measurement system

A non-contact optical measurement procedure is developed to assess the transverse to longitudinal deformation ratio of synthetic

fibres (η_f) - a potential governing parameter in terms of fibre characterization and fibre–matrix interaction optimization -, which is able to measure longitudinal and transverse motion with a single image-capturing device. The methodology described in Section 2.1 assumes the following hypothesis that should be met for accurate displacement estimations.

- The fibre's surface is flat and remains in the same plane parallel to the camera sensor throughout the tensile test. This implies that the sensor and the object surface are parallel and out-of-plane motion of the specimen during loading is negligible. Excessive out-of-plane motion might lead to changes in the magnification of the recorded images and yield additional in-plane displacements.
- The imaging system does not suffer from geometric distortion that impairs the ideal linear correspondence between the physical point and imaged point and produces additional displacements.

2.1. Methodology

2.1.1. Specimen preparation

The basic principle of the digital image correlation is the tracking (or matching) of the same points (or pixels) between two images recorded prior and after deformation. For that, the regions of interest in the fibre's surface must present singular identifiable patterns that can be tracked throughout the tensile test. Usually, this speckle pattern can be the own texture of the specimen or artificially applied by different techniques, these being the spraying and airbrushing of commercial white or black paints on the specimen's surface the most common approach [28–30].

Nowadays, speckle patterns can be readily fabricated for most regular experiments where the region of interest has a size ranging from several millimetres to several meters [30]. However, the small diameter of common synthetic fibres (<1 mm) limits significantly the number of viable and affordable speckle pattern fabrication methods for this application. Effective speckle pattern monitoring for such small surfaces would require costly high-resolution image-capturing devices and/or the reduction of the field of view by placing the lens extremely close to the fibre. This complicates the measurement of crimped fibres, as its surface is not homogeneous and thus, several tensile tests at different locations should be performed to characterize a single fibre or use multiple cameras simultaneously to capture the entire region of interest (length of around 10 mm to include several crimped patterns).

Since full-field surface deformations are not required to determine the average relation between transverse and longitudinal motion of the fibre, an alternative speckle pattern fabrication procedure has been developed to be readily implementable in industrial production systems at a low cost. Different approaches are adopted for the determination of transverse and longitudinal deformations.

Unique high-contrast grayscale patterns to measure transverse deformations are obtained by simply applying a white matt colour to the fibres surface and performing the test in front of a black background. The specimen's edges can be clearly defined by the abrupt change on grayscale intensity between the background region and the fibre's surface. Notice that this approach demands the extension of the analysed region to include part of the background. The approach adopted is schematically depicted in Fig. 1. Fibres that already present light matt colours might not be painted in white when the difference on grayscale intensities with the background is significant.

Several methods have been evaluated to determine the most convenient approach to implement an identifiable pattern for longitudinal displacement measurements in PMFs (Fig. 2). In this case, the main challenge was to introduce an identifiable pattern that would allow the measurement of the longitudinal motion within the same region as the transverse motion with a single image-capturing device. After several tests, it was decided to measure the vertical component of the displacements by painting thin black waved marks along the fibre's length with an ink that will not affect the material being tested (Fig. 4d). Since these marks are painted on the fibre's surface, these deform together with the specimen as a carrier of longitudinal deformation information. The number, location and shape of the marks were carefully assessed in order to avoid measurements in regions close to the anchoring area, interference with the transverse edge detection algorithm and facilitate the identification of unique points in the images before and after loading.

2.1.2. Image acquisition system

The main components of the image acquisition system are shown in Fig. 3. It consists of an Olympus OM-D E-M10 Mark III camera fitted with a M. ZUIKO ED 30 mm 1:3.5 macro lens and an STF-8 macro flash (Fig. 3a). A Benro tripod TGP27A (Fig. 3b) with a Manfrotto 454 micro-positioning sliding plate (Fig. 3c) is used to stabilize and accurately control the distance between the lens and the fibre. To maximize the number of pixels covering the fibre's width in the digital images, the sensor of the camera has to be placed as close as possible to the specimen. The lens selected is specifically used in macro photography due to its large magnification ratio (2.5:1 compared to the typical 1:1 ratios in other macro lenses) and short focusing distance, which allows to place the lens of the camera 4 cm away from the fibre. Fig. 3d shows a close-up of the distance between the specimen and the camera lens.

The camera was placed with its optical axis normal to the specimen surface, imaging the planar specimen surface in different loading states onto its sensor plane. Several trials were performed to define the camera settings (ISO, aperture and shutter speed) and the configuration of the external flash to improve the quality of the digital image. The final settings adopted were ISO 200, aperture f/5.6, shutter speed 1/40 s and intensity of the external flash 1/16. Photos were taken from the unloaded state until failure of the specimen every 1 s. Details on the tensile loading set-up configuration are provided in Section 3.2.

2.1.3. Image processing algorithm

An image processing algorithm coded in the Matlab environment (R-2019a) is developed to analyse the images captured during the tensile test and obtain the relation between transverse and longitudinal deformation of the different fibres evaluated (η_f). The different steps included in the algorithm are described below:

STEP 1: Selection of the region of interest and correction of the fibre inclination

The region of interest must include the 4 marks painted in the fibre and part of the black background. Afterwards, correction of the fibre inclination is performed –if necessary- to assure vertical placement of the fibres. The same procedure is applied to initial and final images analysed. Fig. 4 shows images of the selection and inclination correction process.

STEP 2. Edge detection and location of the marks in the initial and final image

An edge detecting algorithm is applied to identify horizontal and vertical edges based on the Matlab implementation of the Canny method [31]. This computational approach finds edges by

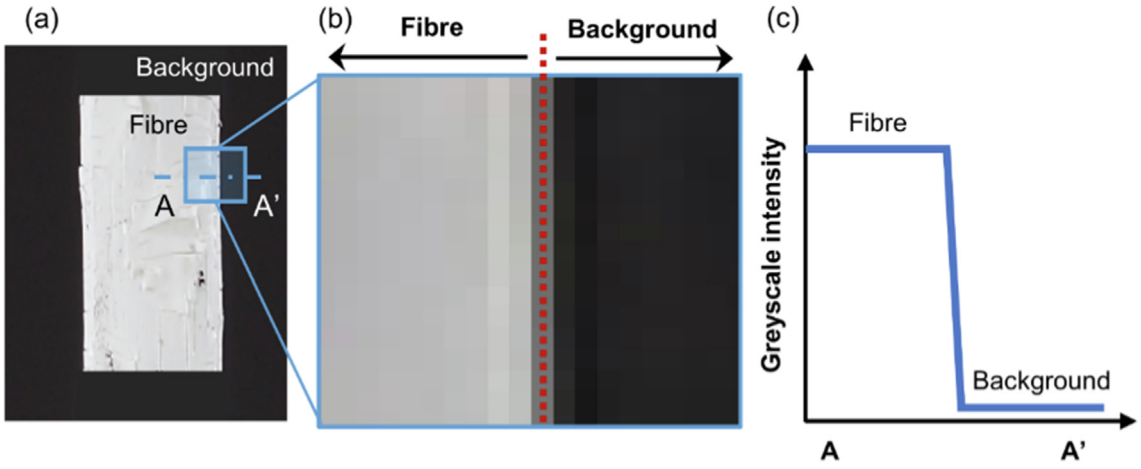

Fig. 1. Schematic representation of (a) White fibre over a black background, (b) Detail of the interface between fibre and background and (c) Changes on greyscale intensity between fibre and background.

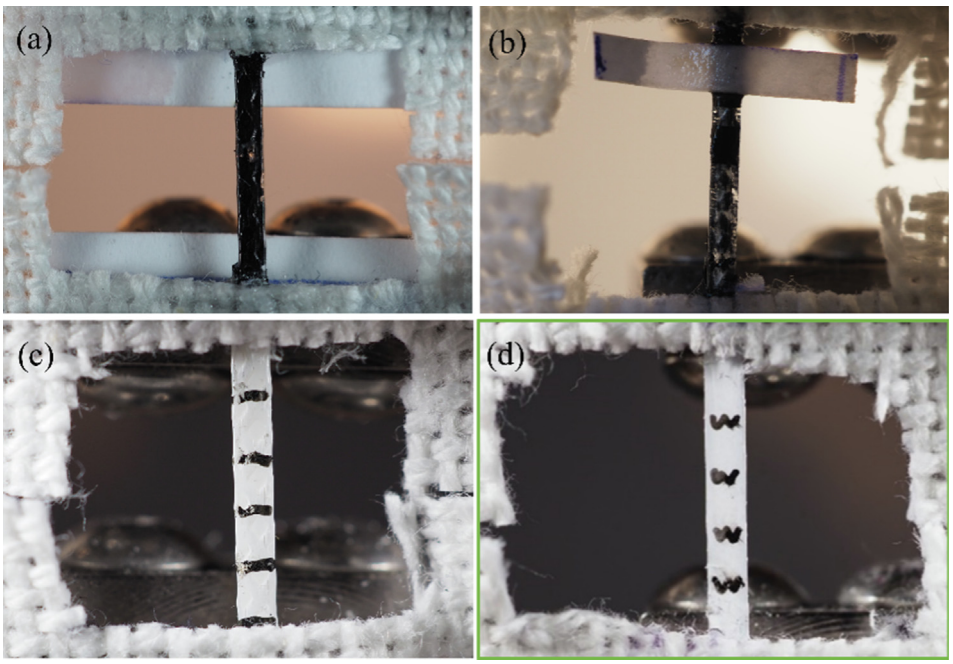

Fig. 2. Identifiable patterns evaluated for vertical displacements. (a) Cardboard on the frame, (b) Cardboard on the fibre, (c) Horizontal marks and (d) Waved marks on the fibre.

searching local maxima of the gradient of the image. The edge function calculates the gradient using the derivative of a Gaussian filter. This method uses two thresholds to detect strong and weak edges, including weak edges in the output if these are connected to strong edges. The threshold values were set to [0.01, 0.09]. The standard deviation of the Gaussian filter was set to 1. The location of upper and lower edges of the 4 marks printed on the fibres are defined by identifying the y-coordinate of the same 4 singular points (pixels) in the initial and final image, as shown in Fig. 5.

STEP 3. Determination of longitudinal deformation

The longitudinal deformation is calculated in the 3 regions between marks (R1, R2 and R3 in Fig. 6) by measuring the distance (in pixels) between the top and bottom edge of the region in image prior and after loading. Areas covered by the marks are not considered in the analysis as these might present distortions caused by the ink. 4 values of longitudinal deformation are obtained within each region. Therefore, the mean value of longitudinal deformation is the average of 12 measurements. This number could be modified based on the particularities of each fibre and set-up adopted to comply with the desired variability of the measurements.

STEP 4. Determination of transversal deformation

RGB (red green blue) images prior and after loading are converted to a binary image by replacing all pixels in the original image with luminance greater than a threshold level with the value 1 (white) and replacing all other pixels with the value 0 (black). The threshold value is determined by minimizing the interclass variance of the black and white pixels through the Otsu's method [32]. The number of pixels covering the width of the fibre are computed for each row within region 1, 2 and 3 (R1, R2 and R3 in Fig. 7) of the images prior (a) and after (b) loading. By this approach, a total of around 700 width measurement are performed along the length of each fibre.

Fig. 3. Image capture system.

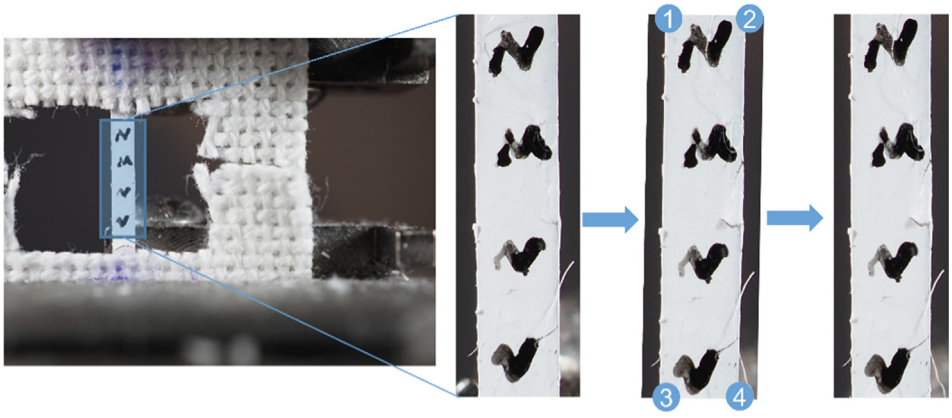

Fig. 4. Selection of the region of interest and correction of fibre inclination.

Transversal deformations are calculated for each row of pixels in the initial image within regions 1, 2 and 3 based on the width variation prior and after loading (Fig. 7c). Since there is an elongation of the fibre, the number of rows covering the initial and final image increases. This could potentially difficult the matching process between images. This ambiguity is commonly referred to as the aperture problem [33]. However, in this application the end points of each region are covered in the analysis. In this case, the motion vector is uniquely determined by considering the longitudinal deformation calculated previously within each region.

Transversal deformations values are filtered by an outlier detection algorithm as some regions of the fibres might present defects caused during the manufacturing process that result in incorrect measurements (Fig. 7d). It is considered an outlier those values that are more than three scaled median absolute deviations (MAD) away from the median.

STEP 5. Determination of the transverse to longitudinal deformation ratio.

The transverse to longitudinal deformation ratio is calculated for all sections within each region with valid (not an outlier) trans-

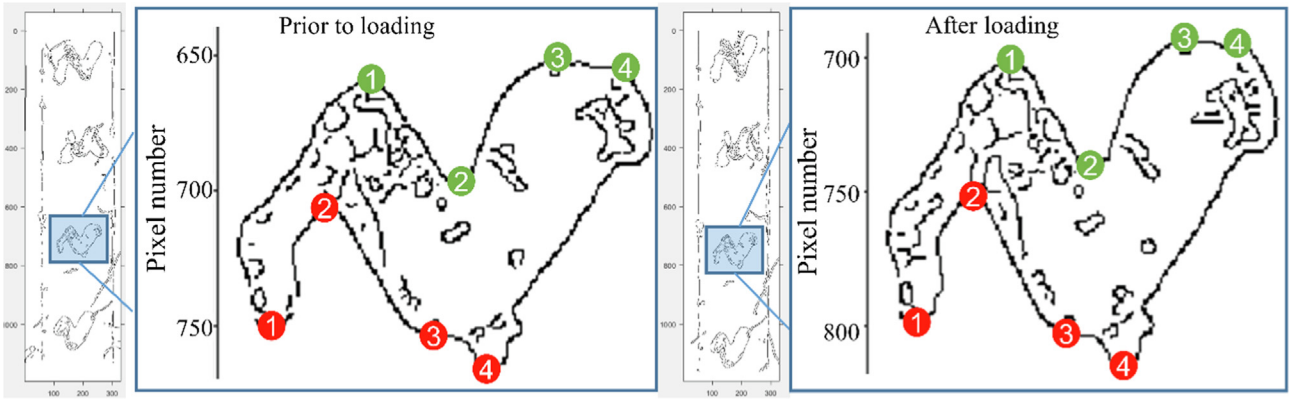

Fig. 5. Location of the same identifiable pixels within the upper and lower edge of each mark prior and after loading.

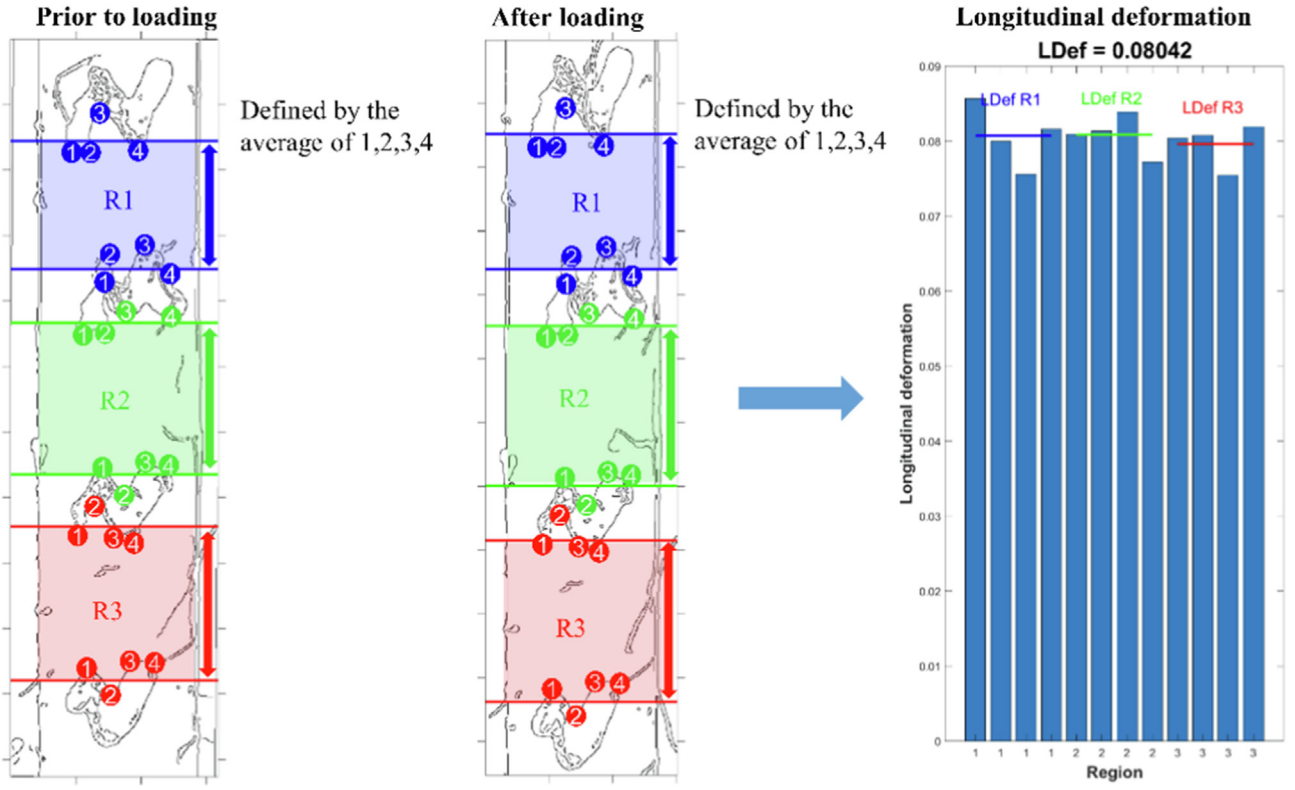

Fig. 6. Longitudinal deformation measurement.

verse deformation measurements (Fig. 8). First, the average lateral deformation in each region is divided by the average longitudinal deformation of the same region. The average of these 3 values is reported as the final transverse to longitudinal deformation ratio. Taking into account the average number of outliers neglected in the analysis of a fibre, the mean value of transverse to longitudinal deformation ratio of each fibre corresponds to the average of around 250 measurements. This value will increase proportionally by the number of replicas tested for each fibre type.

2.2. Validation of longitudinal deformation measurements

Longitudinal deformation values obtained by the proposed optical measurement methodology (Section 2.1) are validated with the axial deformation measured by an external extensometer. Due to initial aperture limitations (50 mm), the extensometer could not be attached on the real fibres evaluated, with an exposed length of just 1 cm. Instead, fibres of 12 cm were prepared following the same process as described in detail in section 3. Fig. 9a shows a sample of the filament tested, which has an exposed length of 7 cm. The deformation process was recorded simultaneously by the image capture system described in section 2.1.2 and the extensometer located on the opposite side (Fig. 9b). Details on the testing conditions adopted are described in section 3.

Fig. 10 presents the load – elongation curves of the 4 tensile tests performed with the axial extensometer attached. The validation of the measurements of the optical method is executed by comparing the longitudinal deformation associated with the first microfilament failure. Fig. 10a identifies these values for the extensometer based on the first slope drop observed in the curves. The

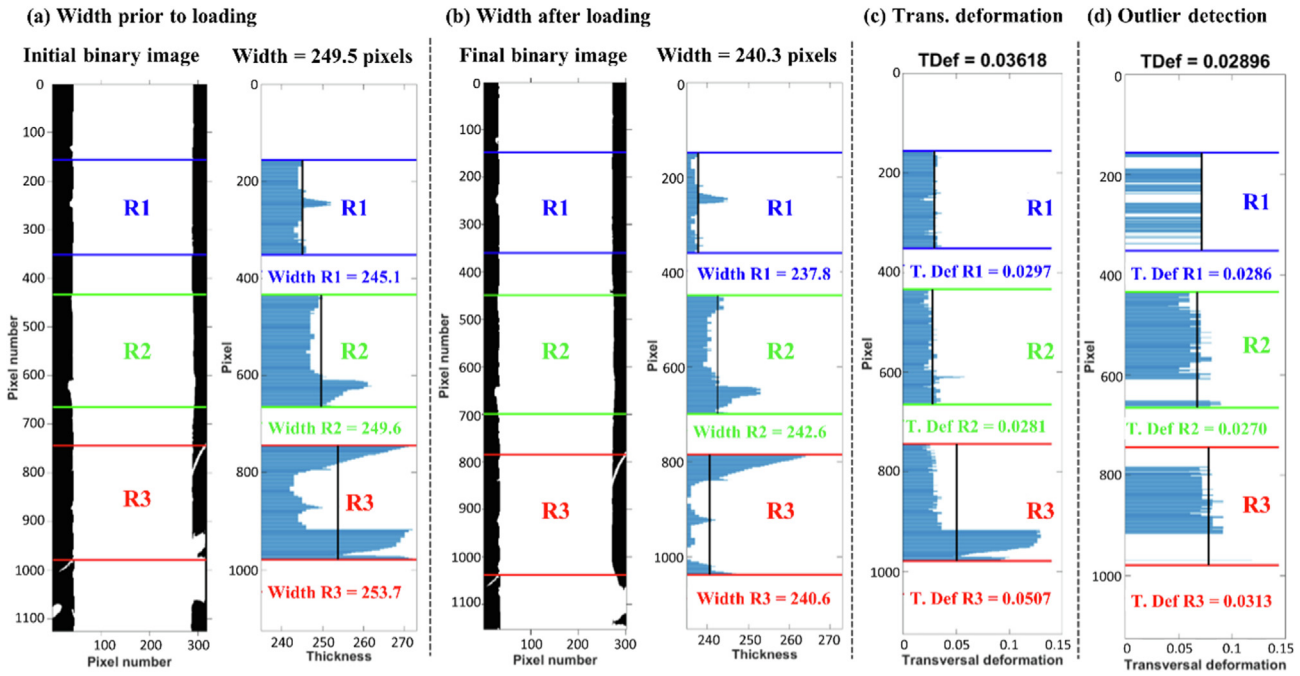

Fig. 7. Measurement of the fibre width prior and after loading.

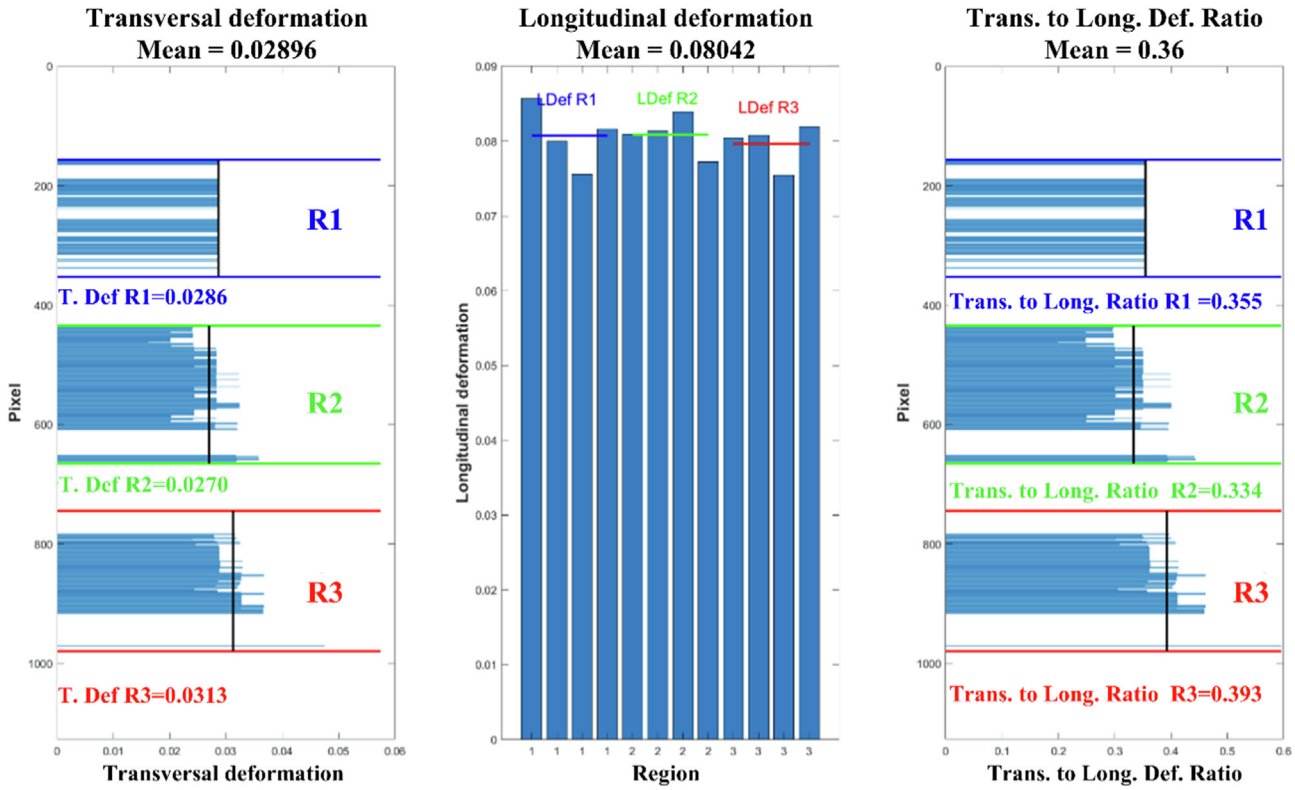

Fig. 8. Transverse to longitudinal deformation ratio measurements.

corresponding image for the optical measurement is selected by visually identifying the first partial failure of the fibre during the tensile test (outlined in green in Fig. 10b). Following failure stages are not considered during the analysis. Table 1 compares the values obtained by the optical measurement technique and the contact extensometer. The error obtained ranged from 0 to 4.5 %, which indicate a good agreement between both methodologies.

3. Materials and test

3.1. Materials: Fibres

A blind cross-wise comparison of plastic fibres (most of which commercially available, other just at lab grade level) was carried out in this manuscript. With this aim, 3 different types of plastic

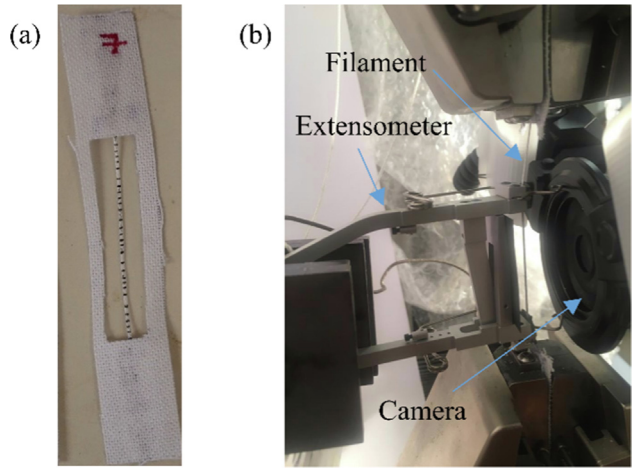

Fig. 9. (a) Filament tested to attach the extensometer and (b) Close-up of the test set-up.

fibres (Polyolefin based fibres, Polyethylene Terephthalate based fibres and Polyvinyl Alcohol based fibres abbreviated as PF, PET and PVA respectively) from 6 different blind suppliers (named A, B, C, D, E and F) with different geometry and texture were tested. A total of 20 synthetic fibres were studied.

The nomenclature used here to refer to each fibre includes the type of plastic fibre (PF, PET and PVA) followed by a letter referring to the blind supplier of the fibre (A to F), back slash, the Length followed by a hyphen and the Equivalent diameter of fibre, back slash, the curvature (calculated as Thickness/Width, 3 curvatures were defined: Low, Medium and High) followed by a hyphen and texture (embossed or un-embossed). For example, PFA/50–0.75/L-U indicates the specimen tested corresponds to a with Polyolefin fibre, supplied by company A with a length and equivalent diameter of 50 and 0.75 respectively with low curvature and an un-embossed texture. The nomenclature adopted, together with the main physical characteristics of the different fibres tested are summarised in Table 2.

3.2. Uniaxial tensile test of plastic fibres

The uniaxial tensile test is the most fundamental test to characterize the mechanical properties of fibres. This is usually performed on long raw filaments to ensure no gripping effects during the test. However, in this research it was deemed representative to characterize the actual products used in fibre reinforced concrete applications and thus, fibres with the real length are evaluated. Despite the complexity and costs associated to this testing procedure, its application is imperative to understand and characterize the material. Different testing configurations have been assessed to ensure reliable and reproducible uniaxial tensile test results for fibres between 40 and 60 mm lengths. Furthermore, it must be highlighted that crack widths in concrete are limited to 0.5 mm in service (owe to durability and performance requirements), hence, the clear length – length not embedded into the concrete matrix – subjected to pull-out force is very short.

After a thorough assessment individual fibres were mounted on textile frames to increase the adhesion and friction between the fibre and the grips of the testing machine based on the methodology presented in [34]. All frames have a central cut-out of 10 mm and variable anchoring lengths depending on the fibre length. Following the recommendations of the American standard ASTM C1557-20 [35], the anchoring length adopted is always greater than 1.5 times the central opening to minimize the gripping effects.

Fig. 11 shows a schematic representation of the textile frame adopted in the present project for a PFB/48–0.94/M-E plastic fibre. It consists of two main elements: a front frame (Fig. 11a) and rear textile plates (Fig. 11b). The fibre is placed between these two elements and fixed with a quick drying cyanoacrylate adhesive. The final configuration of the specimen is illustrated in Fig. 11c. The specific frame dimensions depicted are suitable for fibres with length around 55–60 mm.

The frame was carefully gripped in the clamps of the testing machine (Fig. 12a) ensuring a correct alignment of the fibre. Prior to testing, cuts were made from each side to the central cut-out (red dotted lines of Fig. 11c), ensuring that only the fibre is loaded during the test (Fig. 12b).

For the direct tensile test, an MTS landmark testing machine with 10 kN capacity was used under displacement control mode with pace rate of 0.15 mm/sec (9 mm/min). Prior to test onset, a preload of 10 N was applied. While the load data were taken directly form the load cell, the displacement measurements were taken out of the specimens directly using the aforementioned modified DIC 2D approach (presented in detail in section 2).

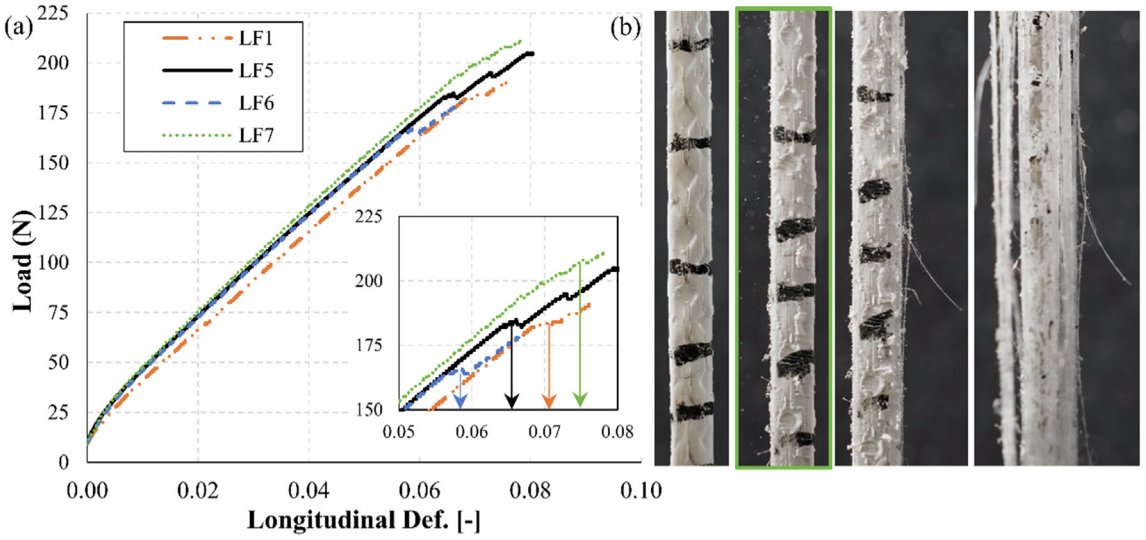

Fig. 10. Validation of longitudinal deformations with the extensometer.

Table 1
Measurement error of the image processing methodology.

Test	Long. Def. Extensometer (–)	Long. Def. Optical method (–)	Error (%)
LF1	0.071	0.071	0.0
LF5	0.066	0.063	4.5
LF6	0.058	0.059	1.7
LF7	0.074	0.075	1.4

4. Results

This section presents the results obtained in the mechanical characterisation and the determination of the η_f of the analysed fibres. These are gathered in two different sub-sections. The first describes the outcomes of the uniaxial tensile tests performed and the latter presents and analyses the outcomes derived from the methodology developed to determine the η_f of PMFs.

4.1. Tensile behaviour characterisation

Fig. 13 depicts the average load-deformation curves obtained for each type of fibre evaluated. Each curve represents the average of 6–8 tests. The results highlight the wide variety of fibres evaluated, in terms of geometrical and morphology characteristics. The different properties of the fibres are reflected on their mechanical performance, such as the maximum tensile load and deformability prior to failure.

The maximum tensile strength reached range between 227.1 and 698.4 MPa. PFA/50–0.75/L-U, PFA/54–0.77/M-E, PFD/40–0.44/L-U and PFC/48–0.99/L-U present values above 600 MPa, whilst the lowest tensile strength was obtained for the PFA/60–0.96/H-U. The coefficients of variation vary between 2.8% and 10.9%. Fibres with superficial embossment present an average maximum strength of 513.3 MPa with a coefficient of variation of 5.8%. On the other hand, unembossed fibres achieved an average tensile strengh of 403.7 MPa with a coefficient of variation of 6.7%. The better mechanical performance of fibres with embossments is to be expected as most (if not all) of these elements are end products commercially available.

Three different failure modes were identified during the tensile tests. In most of the cases, initial partial evidences of local damage of the fibre were observed prior to a complete failure of the specimen, as depicted in Fig. 14a. This initial partial failure can be clearly observed for the last segments of the load-elongation curves of specimens PFA/50-0.75/L-U and PFB/54-0.74/M-E depicted in Fig. 13. Alternatively, PETE/50-1.10/L-U fibres broke into several wider strips (Fig. 14b), where bottle neck effects prior to failure can be observed. Finally, some PVAF/40–0.95/M-E fibres failed at a region near the clamp, which is caused by an out of plane alignment of the specimen at this region (Fig. 14c).

Finally, Table 3 lists the average maximum tensile loads and the variability associated for each type of fibre. Additionally, it includes an estimation of the stiffness of all fibres tested. These values assume a linear behaviour of the material between test onset and failure and that the maximum load reached corresponds to the longitudinal deformation measured by the image analysis algorithm.

4.2. Transverse to longitudinal deformation ratio (η_f) measurement error

Once the tensile behaviour of the fibres evaluated is characterised, it is possible to estimate the measurement error of the methodology described in Section 2.1. Table 4 presents the η_f measurement error for each fibre evaluated. This is estimated based on the ratio between the transverse deformation associated with a **±1** pixel width variation (determined based on the number of pixels covering fibre's width) and the longitudinal deformation developed prior to failure (ε_l in Table 3). The error associated to longitudinal deformation measurements is neglected as the length evaluated of fibre is significantly larger than the width [36].

The optical measurement method presented have a minimum resolution than ranges from 5 to 6 μm in the transverse direction. With this resolution, the error values obtained for the η_f range from 0.005 to 0.118, with a mean value of 0.068. These ranges are above the recommended values for the determination of elastic tensile properties of plastics, which is usually around 0.004 (if considered an expected Poisson ratio of 0.4) [25]. Even though the precision for some rigid and thin fibres evaluated is not ideal, the

Table 2
Main physical characteristics of the fibres studied.

Name	Ref.	Dimensions (mm)				Curvature[2]	Texture
		Length	Width	Thick	$\phi_{eq}^{(1)}$		
PF-A	PFA/50–0.75/L-U	50	2.02	0.30	0.75	Low	Un-embossed
	PFA/40–0.75/H-E	40	1.04	0.70	0.75	High	Embossed
	PFA/48–0.85/H-E	48	1.05	0.67	0.85	High	
	PFA/54–0.77/M-E	54	1.23	0.53	0.77	Medium	
	PFA/56–0.84/M-E	56	1.22	0.45	0.84	Medium	
	PFA/55–0.86/H-U_a	55	0.95	0.61	0.86	High	Un-embossed
	PFA/55–0.86/H-U_b	55	0.93	0.62	0.86	High	
	PFA/60–0.89/H-U	60	1.08	0.58	0.89	High	
	PFA/60–0.88/H-U	60	0.96	0.63	0.88	High	
	PFA/60–0.96/H-U	60	1.17	0.62	0.96	High	
	PFA/45–0.84/H-U	45	0.91	0.61	0.84	High	
	PFA/55–0.81/H-U	55	0.90	0.57	0.81	High	
	PFA/50–0.89/H-U	50	0.94	0.66	0.89	High	
PF-B	PFB/57–0.46/M-E	57.75	1.14	0.38	0.46	Medium	Embossed
	PFB/54–0.74/M-E	54	1.46	0.48	0.74	Medium	
	PFB/48–0.94/M-E	48	1.53	0.50	0.94	Medium	
PF-C	PFC/48–0.99/L-U	48–58	1.58	0.12	0.99	Low	Un-embossed
PF-D	PFD/40–0.44/L-U	40	1.4	0.1	0.44	Low	Un-embossed
PET-E	PETE/50–1.10/L-U	50	2.7	0.35	1.1	Low	Un-embossed
PVA-F	PVAF/40–0.95/M-E	40	1.3	0.55	0.95	Medium	Embossed

[1]Equivalent diameter, calculated by the equation: $\varnothing_{eq} = \sqrt{\frac{4Sectionalarea}{\pi}}$.
[2]Curvature = Thickness/Width. Low (Curvature < 0.15), Medium (0.15 < Curvature < 0.5) and High (Curvature > 0.5).

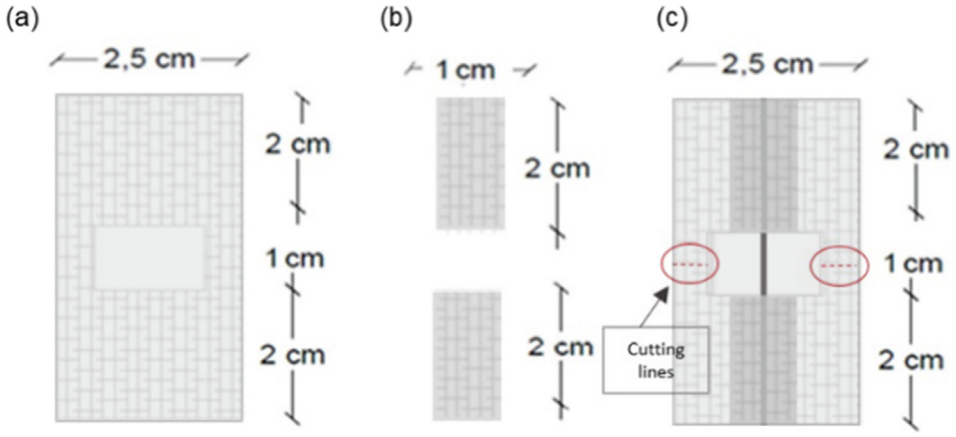

Fig. 11. Textile frame sample (a) front frame dimensions, (b) textile sheets glued on the rear, and (c) fibre glued on the frame and cutting lines.

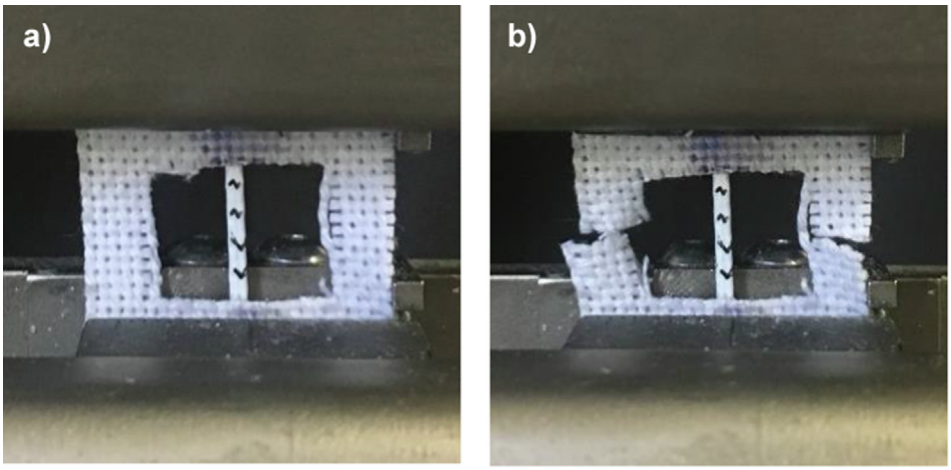

Fig. 12. Tensile test procedure: (a) colocation of the sample, and (b) frame cutting.

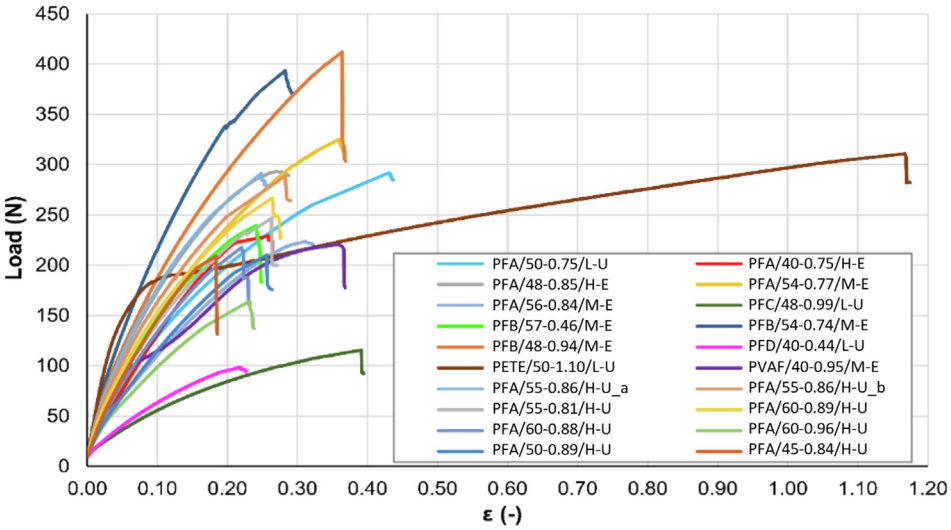

Fig. 13. Load-deformation curves for all the samples analysed.

reliability of the results obtained is compensated with the high number of sections evaluated in each fibre (around 250) and the number of replicas tested (6–8). The final transverse to longitudinal deformation ratio reported for each fibre is the average of 1500–2000 measurements. It is important to remark that the number of fibres tested (and resolution of the image-capturing device used) in this study can be modified for each application to comply with the desired measurement error and statistical variance.

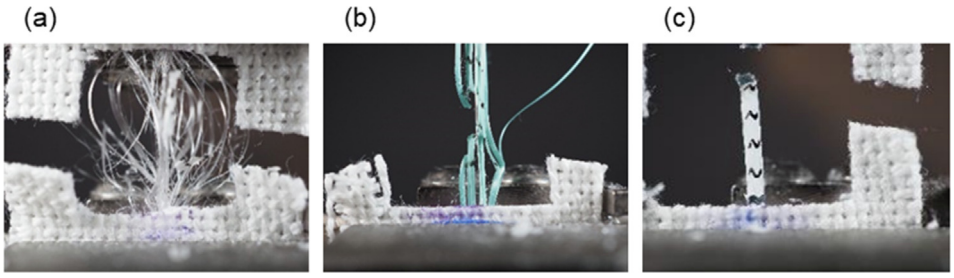

Fig. 14. (a) Typical failure mode, (b) PETE/50–1.10/L-U and (c) PVAF/40–0.95/M-E failure mode.

Table 3
Maximum tensile loads resisted.

Code	Max. load (N)	SD (–)	CV (%)	Stiffness estimation			
				ϕ_{eq}[(1)] (mm)	Strength (MPa)	ε_l[(2)] (–)	E (GPa)
PFA/50–0.75/L-U	291.7	22.4	7.7	0.75	660.3	0.11	5.76
PFA/40–0.75/H-E	229.0	15.5	6.8	0.75	518.3	0.08	6.57
PFA/48–0.85/H-E	291.5	19.3	6.6	0.85	513.7	0.07	7.37
PFA/54–0.77/M-E	325.2	30.0	9.2	0.77	698.4	0.09	7.96
PFA/56–0.84/M-E	224.0	7.5	3.3	0.84	404.2	0.10	4.19
PFA/55–0.86/H-U_a	291.6	31.7	10.9	0.86	502.0	0.06	8.46
PFA/55–0.86/H-U_b	288.8	22.7	7.9	0.86	497.2	0.06	8.21
PFA/60–0.89/H-U	267.0	9.9	3.7	0.89	429.2	0.06	6.92
PFA/60–0.88/H-U	217.9	18.0	8.3	0.88	358.3	0.06	6.51
PFA/60–0.96/H-U	164.4	10.5	6.4	0.96	227.1	0.06	3.87
PFA/45–0.84/H-U	209.3	11.3	5.4	0.84	377.7	0.05	7.36
PFA/55–0.81/H-U	246.9	8.6	3.5	0.81	479.1	0.06	7.84
PFA/50–0.89/H-U	210.1	15.0	7.1	0.89	337.7	0.06	5.33
PFB/57–0.46/M-E	239.8	7.4	3.1	0.74	557.6	0.07	8.52
PFB/54–0.74/M-E	393.7	33.8	8.6	0.94	567.3	0.07	8.08
PFB/48–0.94/M-E	412.0	24.4	5.9	0.99	535.2	0.10	5.14
PFC/48–0.99/L-U	115.6	8.8	7.6	0.46	695.6	0.14	4.83
PFD/40–0.44/L-U	98.7	6.6	6.7	0.44	649.1	0.08	8.59
PETE/50–1.10/L-U	310.8	14.7	4.7	1.1	327.0	0.47	–[(3)]
PVAF/40–0.95/M-E	220.8	6.1	2.8	0.95	311.5	0.14	–[(3)]

(1) Equivalent diameter, calculated by the equation: $\varnothing_{eq} = \sqrt{\frac{4 Sectionalarea}{\pi}}$.
(2) Longitudinal deformation at failure, measured by image analysis.
(3) Not estimated due to a clear bi-linear mechanical behaviour.

Table 4
η_f measurement error.

Fibre	Pixels covering fibre's width	Trans. Def. resolution (–)	Long. Def. at failure (–)	η_f resolution (–)
PFA/50–0.75/L-U	343	0.00292	0.11442	0.025
PFA/48–0.85/H-E	179	0.00559	0.06968	0.080
PFA/56–0.84/M-E	205	0.00488	0.09656	0.051
PFA/54–0.77/M-E	214	0.00467	0.08769	0.053
PFA/55–0.86/H-U_a	174	0.00575	0.05931	0.097
PFA/55–0.86/H-U_b	165	0.00606	0.06059	0.100
PFA/60–0.89/H-U	188	0.00532	0.06201	0.086
PFA/60–0.88/H-U	168	0.00595	0.05501	0.108
PFA/60–0.96/H-U	207	0.00483	0.05868	0.082
PFA/45–0.84/H-U	165	0.00606	0.05132	0.118
PFA/55–0.81/H-U	157	0.00637	0.06111	0.104
PFA/50–0.89/H-U	181	0.00552	0.06331	0.087
PFC/48–0.99/L-U	280	0.00357	0.14405	0.025
PFB/54–0.74/M-E	252	0.00397	0.07019	0.057
PFB/57–0.46/M-E	203	0.00493	0.06541	0.075
PFA/40–0.75/H-E	166	0.00602	0.07834	0.077
PVAF/40–0.95/M-E	227	0.00441	0.14186	0.031
PETE/50–1.10/L-U	430	0.00233	0.47260	0.005
PFB/48–0.94/M-E	266	0.00376	0.10409	0.036
PFD/40–0.44/L-U	245	0.00408	0.07559	0.054

4.3. Transverse to longitudinal deformation ratio (η_f) determination

Digital images captured during the tensile test were analysed with the image processing algorithm described in Section 2.1.3. Unfortunately, the resolution provided by the methodology does not allow the monitoring of the deformation ratio evolution with the load. Instead, the η_f is measured at the axial strain range developed between the test onset and the first partial failure of the fibre.

As a result, the η_f of the fibres estimated is not intended to characterize an elastic property, but rather to provide the average behaviour until failure of the samples. The loss of linearity of the stress to strain curve is not assumed as a termination criterion as the image-capturing device used could not provide sufficient resolution at such low axial strain ranges. In those fibres that experience sufficient transverse deformation to not compromise the accuracy of the results (width reductions above 8 pixels), an additional η_f is determined between the test onset and half of the axial strain range at failure. Fig. 15 depicts a schematic representation of the axial strain region covered by both the η_f until failure and half strain range.

Fig. 16 presents the η_f of the 20 fibres analysed. The nomenclature used for the fibres is described in section 4. The error bars included in each column correspond to a +1/−1 standard deviation. The mean values of η_f at failure and half strain range from 0.34 to 0.88 and from 0.37 to 0.88, respectively. The mean coefficients of variation of the measurements are 9.10 and 11.12 % for failure and half strain conditions, respectively. The generally low variability of the results indicate that the measurements are reliable and that most of the differences observed amongst fibres are statistically significant.

The η_f that characterizes half of the strain range developed until partial failure presents slightly higher mean values and variability than the η_f covering the entire axial elongation until partial failure. The higher variability of the first is explained by the lower transversal deformations developed from the test onset, which translates into an increase of measurement error. Despite the differences are minor, the trends on the mean values reported suggest that the transverse to axial deformation ratio decreases with tensile elongation. Several authors have studied the effects of axial elongation on the Poisson's coefficient of polymeric materials [37–41], obtaining differing results. Refs. [37,38] reported decreases of Poisson's ratio with axial elongation, which was attributed to the start of void formation. On the other hand, [39–41] report an increase of Poisson ratio at higher axial strain values for different thermoplastics due to its viscoelastic behaviour.

Transverse to longitudinal deformation ratios above 0.5 would be a physically incompatible material according to material's thermodynamics fundamental laws. Likewise, typical Poisson's ratios reported in the literature for isotropic elastic polymers range from 0.30 to 0.49 depending on the material composition and testing conditions (e.g., loading rates, temperature, humidity) [42–44], values around 0.40 being the most commonly reported for polypropylene at room temperature [44]. Poisson's ratios above 0.5 can only be attained for anisotropic elastic polymer composites in a particular direction, as orthotropic materials can have unbounded Poisson's ratios [45].

However, it is important to notice that these values were obtained through standardized tests performed within linear axial strain ranges on suitable specimens that comply with certain geometries and surface conditions (ISO 527 [25] and ASTM D638 – 14 [1]). Usually, tensile tests for Poisson's ratio determination are performed on standard dumbbell-shaped specimens of much larger sizes prepared by machining operations, die cutting or injection moulding. All surfaces of the specimen must be flat and free of visible flaws, scratches, or imperfections.

These conditions differ significantly from most of the fibres tested for this experimental program. As described in Table 2, 40% of the fibres evaluated are embossed with medium or high section curvature, 45% are unembossed with medium or high section curvature and only the remaining 15% present flat surfaces. In this context, the η_f derived from the tests carried out with the proposed measurement configuration should not be directly compared with those Poisson's ratio reported in the literature, since different mechanisms -governed by both material mechanical properties and fibre geometry and treatments- might take place in embossed and curved fibres under tensile loading.

4.3.1. Flat unembossed fibres

Fig. 17 highlights the transverse to longitudinal deformation ratios obtained for the unembossed specimens with low section curvature (PETE/50-1.10/L-U; PFA/50-0.75/L-U; PFD/40-0.44/L-U; PFC/48-0.99/L-U) and includes a detail of the specimen's surface. As can be seen, values obtained range from 0.34 to 0.42 and from 0.37 to 0.46 for failure and half strain conditions, respectively. Such results are in agreement with the typical Poisson's ratio reported in the literature for isotropic polyolefin and polyethylene terephthalate materials at room temperature, as these specimens present similar surface characteristics than the standardized specimens used for the Poisson's ratio determination [41].

The measurements performed in these fibres are significantly more consistent than in the other fibres evaluated, with a 50% reduction on the mean coefficient of variation. This behaviour is attributed to the large width and low thickness that present all 4 specimens evaluated in this category. The ratio width/thickness of these fibres range from 6.7 to 14, which is about 4–9 times larger than the other fibres evaluated.

4.3.2. Unembossed fibres with high section curvature

The unembossed fibres with high section curvature (PFA/60-0.96/H-U; PFA/50-0.89/H-U, PFA/55-0.86/H-U_a; PFA/55-0.81/H-U, PFA/55-0.86/H-U_b; PFA/60-0.88/H-U, PFA/60-0.89/H-U and PFA/45-0.84/H-U) are represented in Fig. 18. These also present average values of the η_f within the typical ranges of material Poisson's ratios reported in the literature (average of 0.44). The only exception is the fibre PFA/60-0.96/H-U, with a mean η_f above 0.50.

Despite the uniform section characteristics of these fibres along the monitored length, the high curvature of the surface challenge the hypothesis described in Section 2 for accurate displacement estimations. The surface curvature might introduce out of plane motions that alter the relation between transverse and axial deformations. Moreover, the surface curvature of the specimens might compromise the precision of the measurements, as the distance to the lens varies slightly between the centre and the edges of the fibres. These effects combined are reflected on the variability of the measurements (average coefficient of variation of 10%), as this set of fibres almost double the coefficient of variation of the unembossed specimens with low section curvature.

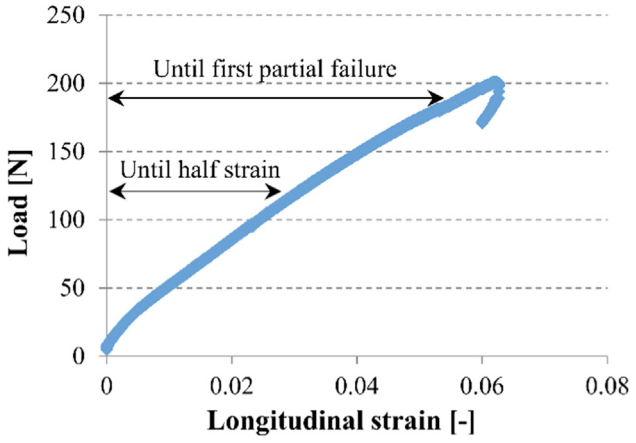

Fig. 15. Strain region covered by each transverse to longitudinal deformation ratio measured.

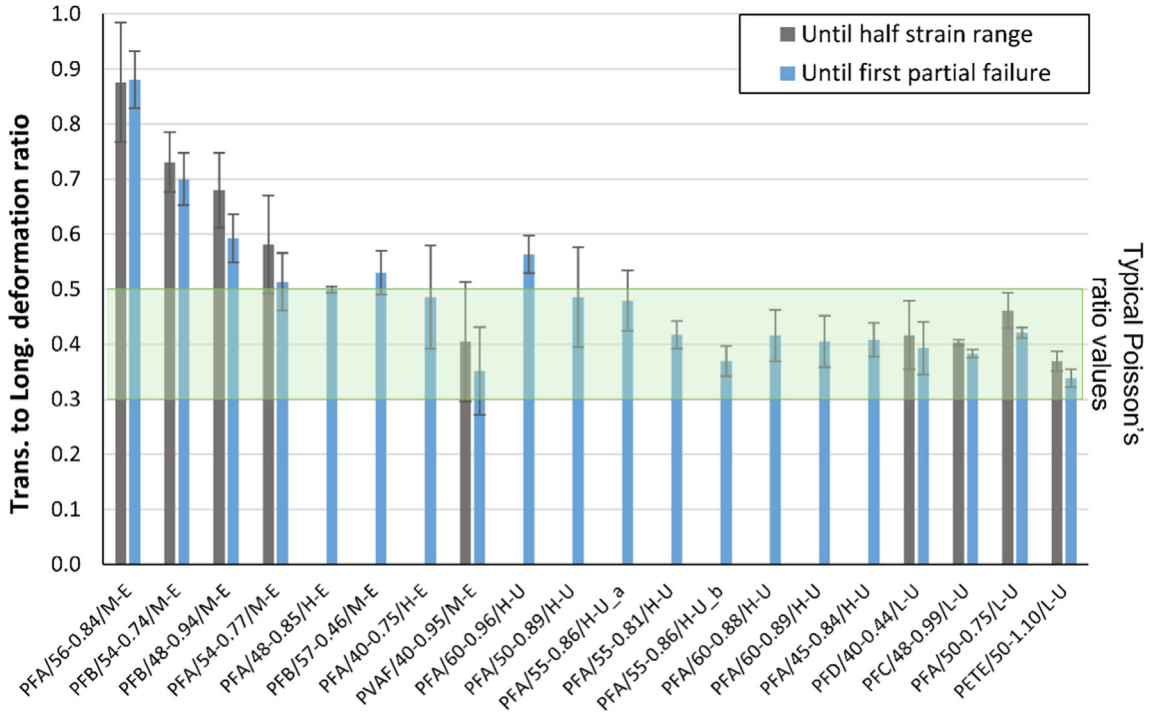

Fig. 16. η_f of the synthetic fibres assessed.

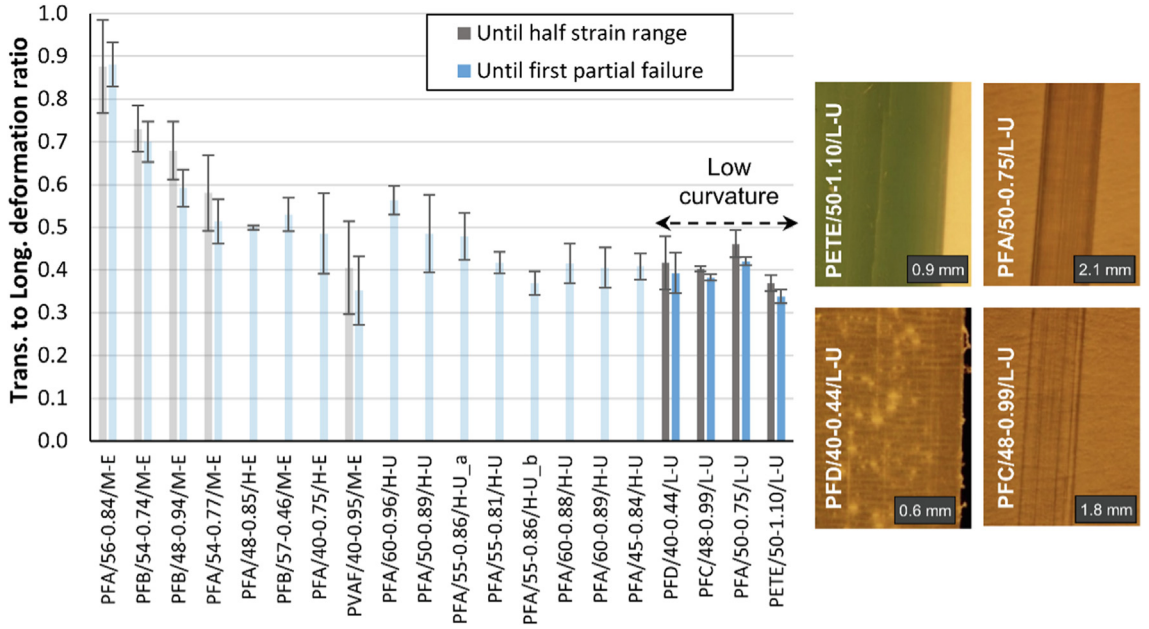

Fig. 17. η_f of the unembossed low curvature fibres.

4.3.3. Embossed fibres

Structural fibres are usually subjected to superficial treatments to introduce geometric irregularities to enhance the adherence between the fibre and the concrete matrix. The intensity of these treatments vary amongst the embossed fibres evaluated. Fig. 19 highlights the η_f obtained for the embossed fibres. The results show large variations amongst the fibres evaluated (from 0.35 to 0.88). The larger values correspond to the fibres with the most intense embossment patterns while the lower values are obtained in the fibres with less intense surface patterns. As explained earlier in the Section 4.3, the η_f measured here capture a different phenomenon than the standardized Poisson's ratio tests. Therefore, the results reported should not be analysed based on the same criteria.

To further analyse this phenomenon, Fig. 20 depicts the width variation and transversal deformation associated to tensile loading of a fibre with intense embossment obtained by the image processing algorithm (PFA/56-0.84/M-E). Even though at plain sight the fibre's width might seem to be uniform, Fig. 20a shows significant initial width variations along the length caused by the embossment treatments. Width at peak regions increases up to the 13 % compared with the width at valley areas. Fig. 20b shows the width

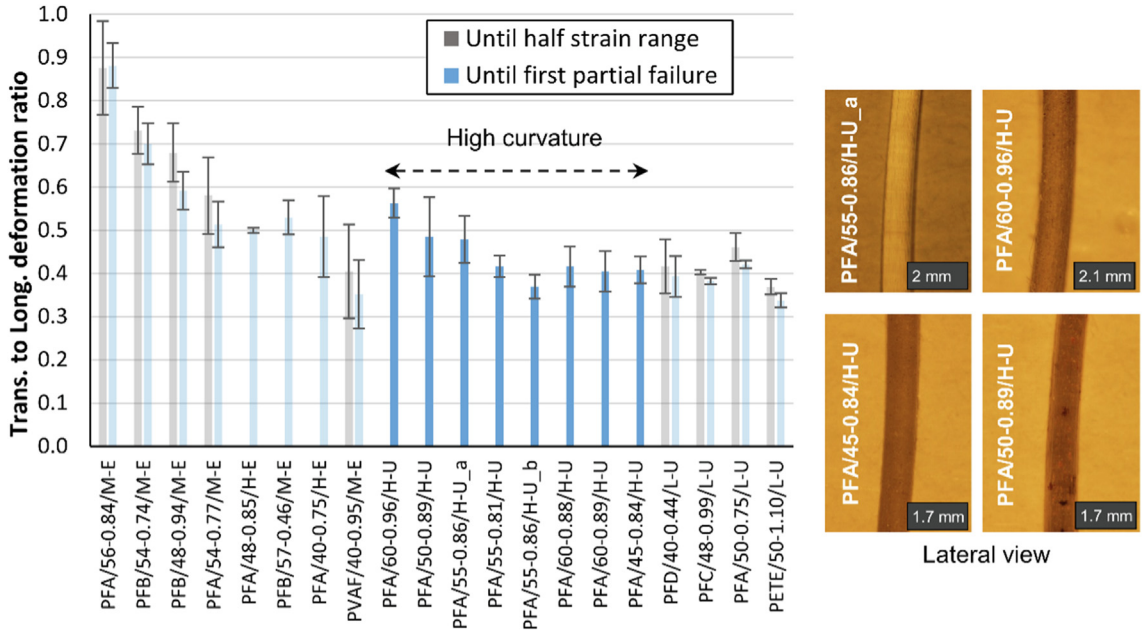

Fig. 18. η_f of the unembossed high curvature fibres.

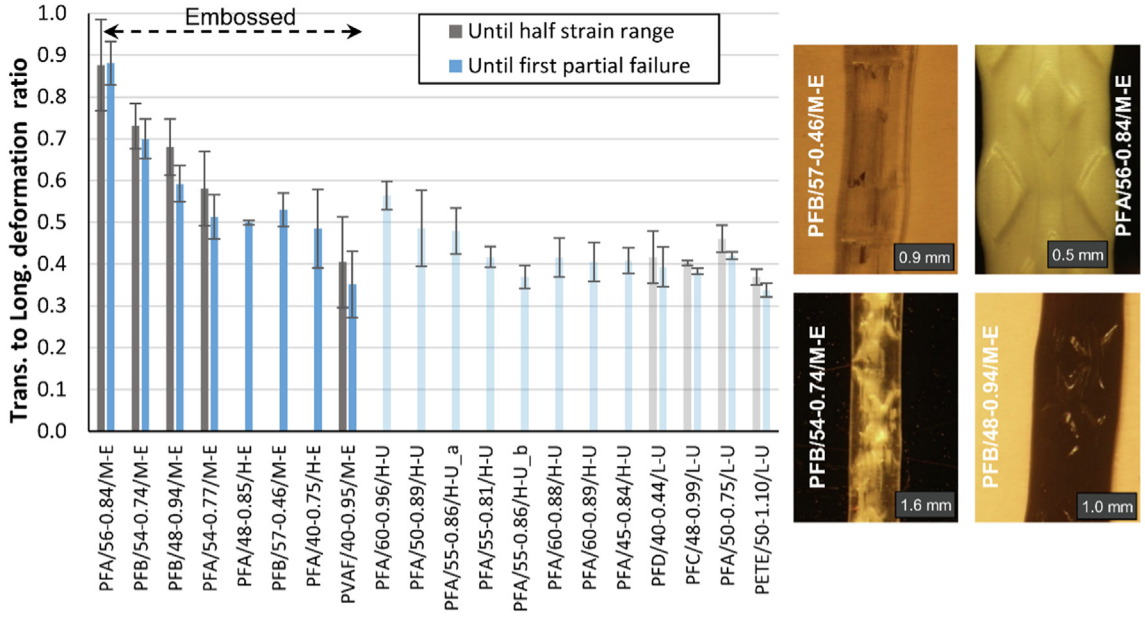

Fig. 19. Transverse to longitudinal deformation ratio of embossed fibres.

distribution after loading. In this case, the fibre's width is more uniform, with the peak and valley regions less clearly identified.

These results suggest that the transversal deformation during tensile loading is non-uniform along the fibre's length when embossment treatments are applied, as the peak regions undergo larger width reductions (Fig. 20c). This behaviour can be explained by the non-uniform material distribution generated by the embossment, which causes a differential alteration of the mechanical properties along the fibre. During axial elongation, the polymeric chains tend to re-align towards the principal tensile stress field induced by the applied load, which leads to this increased non-uniform transverse motion. The magnitude of this transverse contraction is found to be governed by the fibre material and the both the fibre geometry and the embossment pattern applied.

The larger lateral contraction rate experienced by crimped fibres over flat/smooth samples might seem to contradict the practical evidence that crimped fibres perform better than flat/smooth fibres in reinforced cement-based composites. However, it is important to remark that bond strength with cement-based matrices is determined not only by lateral contraction but also by mechanical interlock and, in some cases, chemical adherence. The results obtained here suggest that in most fibre reinforced concretes, physical interlock provided by the crimped patterns dominates over the lateral contraction on the mechanical response of the matrix-fibre interaction during tensile loading, which is in agreement with the results provided by Garnevičius et al. [46].

Notice that depending on the number of peaks and valleys covered within the regions analysed, the transversal deformation

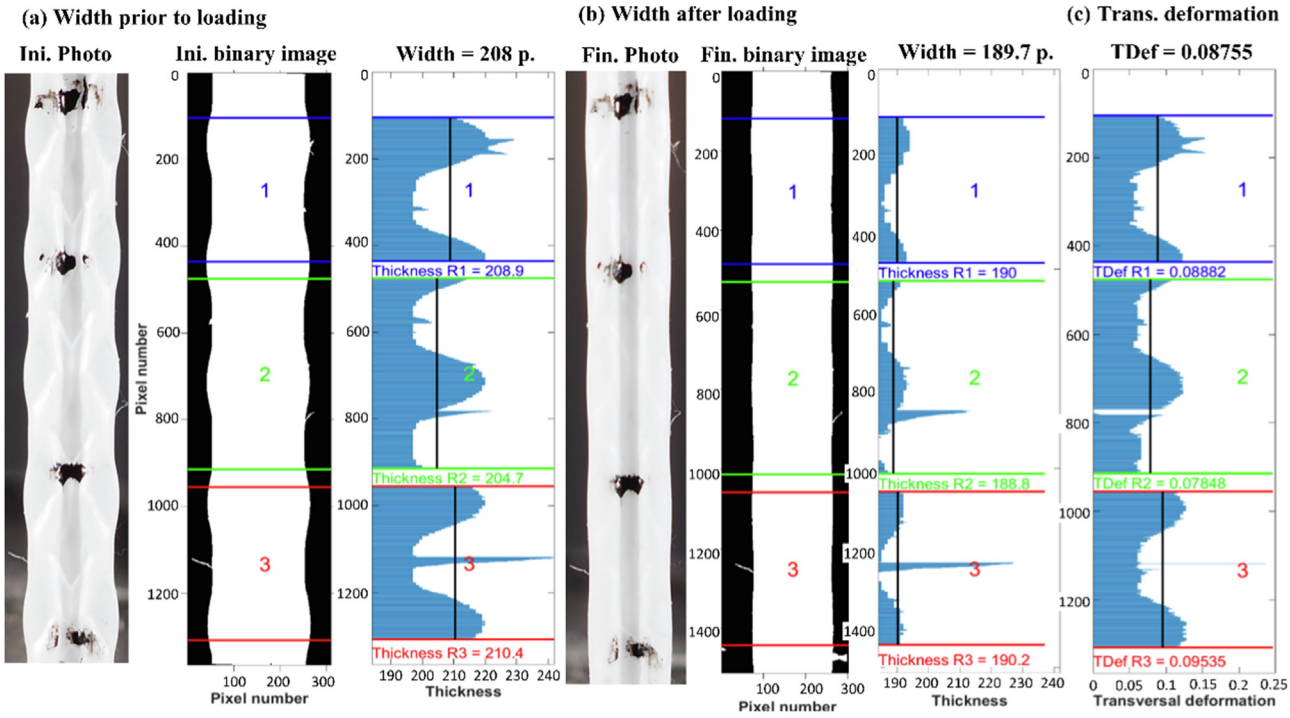

Fig. 20. (a) Initial thickness, (b) Final thickness and (c) Transversal Deformation of PFA/56-0.84/M-E.

obtained might vary significantly, as peaks undergo larger width reductions than valley regions. This explains the larger variability of the measurements obtained in some embossed fibres.

Other sources of variability detected are highlighted in Fig. 21, which specially affects the fibres PFA/40-0.75/H-E and PVAF/40-0.95/M-E. As depicted in the lateral view of the fibre included in Fig. 21, the initial shape of fibre PFA/40-0.75/H-E induces out-of-plane motion during tensile loading as not all sections of the fibre are aligned with the load. Moreover, not all sections are on the same plane parallel to the camera sensor. As a result, pixels covering areas closer to the camera do not represent the same unit dimension than pixels on more distant regions.

On the other hand, PVAF/40-0.95/M-E have a significant presence of what seems to be cutting or moulding wastes randomly distributed on the edges of the fibre (see Fig. 21). Unlike other fibres analysed, these defects are not isolated in a few locations but are present in a significant fraction of the fibre's length. Even though the outlier detection algorithm identifies and disregard the areas affected by the defects, the large presence disrupts the numerical analysis and increases significantly the variability of the measurements.

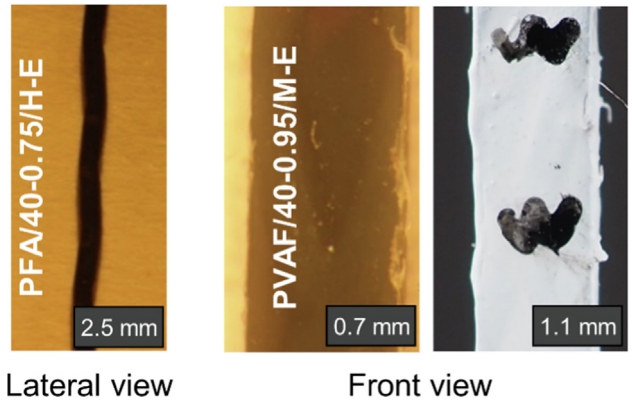

Fig. 21. Other sources of variability detected in embossed fibres.

5. Conclusions

This paper describes a new methodology developed to assess the transverse to longitudinal deformation ratio (η_f) of polymeric macro-fibres with a single image capturing device based on a modified 2D Digital Image Correlation method. The method proposed was validated through an extensive experimental program on 20 selected lab grade and commercial fibres. The main conclusions derived from the experimental tests results and analyses are the following.

- Longitudinal deformations obtained by means of the new DIC procedure differ from extensometer readings by <3.1%, this being a suitable accuracy for the purpose.
- The η_f values obtained for unembossed fibres with flat in-plane straight profiles range from 0.34 to 0.46. Such results are in agreement with the common values reported of Poisson's ratio (ν_f) for standardized isotropic polyolefin and polyethylene terephthalate specimens at room temperature.
- The η_f values for unembossed fibres with high curvature sections range from 0.37 to 0.56, with a mean value of 0.44. In this case, some of the results are inconsistent with the standardized ν_f values reported in the literature for similar materials (always below 0.5). This is attributed to the out-of-plane motion experienced during tensile elongation caused by the high curvature of the fibre's surface and the low accuracy of the measurements for this set of thin rigid fibres. Nonetheless, for qualitative comparison purposes, the η_f values obtained could be a valid reference.
- Fibres with width variations caused by superficial treatments led to η_f values between 0.34 (fibres with less intense surface patterns) to 0.88 (fibres with the most intense embossment pat-

terns). In this case, the wide ranges obtained are not due inaccuracies of the measurement method used. Instead, these results suggest that superficial embossments might alter the effective relation between transverse and axial deformation during tensile elongation, even for fibres with the same material composition. The shrinkage of this range of η_f for fibres with superficial treatment could lead to improvements of the post-cracking response of the PMFRC (i.e., reduction of the variability of the residual flexural strength).

- Despite all η_f reported for each fibre represent the mean of more than 1500 values, the results obtained should be validated with image capturing devices of higher resolution. These should provide an accuracy on the transverse to longitudinal deformation ratio of 1%.

The method proposed herein is aimed at facilitating the characterization of the fibre's transverse to longitudinal deformation ratio (η_f), which is a relevant parameter in fibre–matrix interaction phenomena. Due to the hypotheses assumed and the testing configuration, the ratio η_f experimentally obtained is not necessarily coincident with the fibre ν_f. Nonetheless, for both qualitative comparison of fibres and fibre design-optimization purposes, η_f could be a representative parameter. To verify this statement, further experimental evidences –including fibre pull-out tests on cement-based matrices– are deemed necessary.

6. Data availability

The raw/processed data required to reproduce these findings cannot be shared at this time as the data also forms part of an ongoing study.

Declaration of Competing Interest

The authors declare that they have no known competing financial interests or personal relationships that could have appeared to influence the work reported in this paper.

Acknowledgements

T. Ikumi is supported by the Torres Quevedo programme PTQ2018-009877 sponsored by the Spanish Ministry of Science and Innovation. The authors also express their gratitude to the same Spanish Ministry for the financial support received under the scope of the project CREEF (PID2019-108978RB-C32). Finally, the authors acknowledge the support of Catalan agency AGAUR through their research groups' support programme (2017SGR00227 and 2017SGR01481).

References

[1] ASTM D638-14, Standard Test Method for Tensile Properties of Plastics, 2014.
[2] D.C. Hughes, Stress transfer between fibrillated polyalkene films and cement matrices, Composites 15 (2) (1984) 153–158.
[3] M.R. Piggott, Debonding and friction at fibre-polymer interfaces. I: Criteria for failure and sliding, Compos. Sci. Technol. 30 (4) (1987) 295–306.
[4] A. Bentur, S. Mindess, Fibre Reinforced Cementitious Composites, Crc Press, 2007.
[5] J.K. Kim, Y.W. Mai, B. Cotterell, WS9a2 – The effect of fibre pre-tension on residual stresses in fibre composites, Mech. Behav. Mater. VI, Pergamon (1992) 11–16, https://doi.org/10.1016/B978-0-08-037890-9.50255-6.
[6] A. Bentur, S. Mindess, G. Vondran, Bonding in polypropylene fibre reinforced concretes, Int. J. Cem. Compos. Lightweight Concr. 11 (3) (1989) 153–158.
[7] R. Baggott, D. Gandhi, Multiple cracking in aligned polypropylene fibre reinforced cement composites, J. Mater. Sci. 16 (1) (1981) 65–74.
[8] J.R. Roesler, S.A. Altoubat, D.A. Lange, K.A. Rieder, G.R. Ulreich, Effect of synthetic fibers on structural behavior of concrete slabs-on-ground, ACI Mater. J. 103 (2006) 3–10.
[9] A. Conforti, G. Tiberti, G.A. Plizzari, A. Caratelli, A. Meda, Precast tunnel segments reinforced by macro-synthetic fibers, Tunn. Undergr. Sp. Technol. 63 (2017) 1–11, https://doi.org/10.1016/j.tust.2016.12.005.
[10] P. Pujadas, A. Blanco, S. Cavalaro, A. de la Fuente, A. Aguado, The need to consider flexural post-cracking creep behavior of macro-synthetic fiber reinforced concrete, Constr. Build. Mater. 149 (2017) 790–800, https://doi.org/10.1016/j.conbuildmat.2017.05.166.
[11] P. Pujadas, A. Blanco, S. Cavalaro, A. de la Fuente, A. Aguado, Fibre distribution in macro-plastic fibre reinforced concrete slab - panels, Constr. Build. Mater. 64 (2014) 496–503, https://doi.org/10.1016/j.conbuildmat.2014.04.067.
[12] P. Pujadas, A. Blanco, S. Cavalaro, A. Aguado, Plastic fibres as the only reinforcement for flat suspended slabs: experimental investigation and numerical simulation, Constr. Build. Mater. 57 (2014) 92–104.
[13] Z. Deng, X. Liu, P. Chen, A. Fuente, X. Zhou, N. Liang, Y. Han, L. Du, Basalt-polypropylene fiber reinforced concrete for durable and sustainable pipe production. Part 1: Experimental program, Struct. Concr. 23 (1) (2022) 311–327, https://doi.org/10.1002/suco.202000759.
[14] Z. Deng, X. Liu, P. Chen, A. Fuente, Y. Zhao, N. Liang, X. Zhou, L. Du, Y. Han, Basalt-polypropylene fiber reinforced concrete for durable and sustainable pipe production. Part 2: Numerical and parametric analysis, Struct. Concr. 23 (1) (2022) 328–345, https://doi.org/10.1002/suco.202000760.
[15] A. de la Fuente, R.C. Escariz, A.D. de Figueiredo, A. Aguado, Design of macro-synthetic fibre reinforced concrete pipes, Constr. Build. Mater. 43 (2013) 523–532, https://doi.org/10.1016/j.conbuildmat.2013.02.036.
[16] S. Lee, Y. Park, A. Abolmaali, Investigation of flexural toughness for steel-and-synthetic-fiber-reinforced concrete pipes, Structures 19 (2019) 203–211.
[17] D. Martinello, S.H.P. Cavalaro, A. de la Fuente, Flexural fatigue of pre-cracked plastic fibre reinforced concrete: experimental study and numerical modelling, Cem. Concr. Compos. 2021. doi.org/10.1016/j.cemconcomp.2020.103850.
[18] O. Pons, M.M. Casanovas-Rubio, J. Armengou, A. de la Fuente, Sustainability-driven decision-making model: case study of fiber-reinforced concrete foundation piles, J. Constr. Eng. Manage. 147 (10) (2021), https://doi.org/10.1061/(ASCE)CO.1943-7862.0002073.
[19] M.G. Alberti, C.G. Jaime, A. Enfedaque, A. Carmona, C. Valverde, G. Pardo, Use of Steel and Polyolefin Fibres in the La Canda Tunnels: Applying MIVES for Assessing Sustainability Evaluation, 2018. pp. 1–11. <https://doi.org/10.3390/su10124765>.
[20] T. Ikumi, E. Galeote, P. Pujadas, A. de la Fuente, R.D. López-Carreño, Neural network-aided prediction of post-cracking tensile strength of fibre-reinforced concrete, Comput. Struct. 256 (2021) 106640, https://doi.org/10.1016/j.compstruc.2021.106640.
[21] A. de la Fuente, M.D.M. Casanovas-Rubio, O. Pons, J. Armengou, Sustainability of column-supported RC slabs: fiber reinforcement as an alternative, J. Constr. Eng. Manage. 145 (7) (2019), https://doi.org/10.1061/(ASCE)CO.1943-7862.0001667.
[22] A. de la Fuente, O. Pons, A. Josa, A. Aguado, Multi-criteria decision making in the sustainability assessment of sewerage pipe systems, J. Clean. Prod. 112 (2016) 4762–4770, https://doi.org/10.1016/j.jclepro.2015.07.002.
[23] A. de la Fuente, A. Blanco, J. Armengou, A. Aguado, Sustainability based-approach to determine the concrete type and reinforcement configuration of TBM tunnels linings. Case study: extension line to Barcelona Airport T1, Tunnell. Undergr. Space Technol. 61 (2017) 179–188, https://doi.org/10.1016/j.tust.2016.10.008.
[24] A. Meza, P. Pujadas, L.M. Meza, F. Pardo-Bosch, R.D. López-Carreño, Mechanical optimization of concrete with recycled pet fibres based on a statistical-experimental study, Materials 14 (2) (2021) 240.
[25] ISO 527-1, Plastics. Determination of tensile properties. Part 1: General principles, 2019.
[26] A.J.W. McClung, G.P. Tandon, K.E. Goecke, J.W. Baur, Non-contact technique for characterizing full-field surface deformation of shape memory polymers at elevated and room temperatures, Polym. Test. 30 (1) (2011) 140–149.
[27] R.H. Pritchard, P. Lava, D. Debruyne, E.M. Terentjev, Precise determination of the Poisson ratio in soft materials with 2D digital image correlation, Soft Matter 9 (26) (2013) 6037, https://doi.org/10.1039/c3sm50901j.
[28] Y.L. Dong, B. Pan, A review of speckle pattern fabrication and assessment for digital image correlation, Exp. Mech. 57 (8) (2017) 1161–1181.
[29] J. Park, S. Yoon, T.-H. Kwon, K. Park, Assessment of speckle-pattern quality in digital image correlation based on gray intensity and speckle morphology, Opt. Lasers Eng. 91 (2017) 62–72.
[30] B. Pan, K. Qian, H. Xie, A. Asundi, Two-dimensional digital image correlation for in-plane displacement and strain measurement: a review, Meas. Sci. Technol. 20 (6) (2009) 062001, https://doi.org/10.1088/0957-0233/20/6/062001.
[31] J. Canny, A computational approach to edge detection, IEEE Trans. Pattern Anal. Mach. Intell. PAMI-8 (6) (1986) 679–698.
[32] N. Otsu, A threshold selection method from gray-level histograms, IEEE Trans. Syst. Man Cybern. 9 (1) (1979) 62–66.
[33] F. Sur, B. Blaysat, M. Grédiac, On biases in displacement estimation for image registration, with a focus on photomechanics, J. Math. Imag. Vis. Springer Verlag 63 (7) (2021) 777–806.
[34] A.R.E. Cáceres, I. Galobardes, A.D.d. Figueiredo, Mechanical characterization of synthetic macrofibres, Mater. Res. 19 (3) (2016) 711–720.
[35] America Society for Testing Materials, ASTM C1557–20: Standard Test Method for Tensile Strength and Young's Modulus for Fibres, ASTM, West Conshohocken, PA, 2020.
[36] Z. Hu, H. Xie, T. Hua, Z. Wang, Advanced intensity correlation method for evaluating poisson's ratio of fibrelike material, Rev. Sci. Instrum. 80 (2009).

[37] K. Higuchi, H. Takai, Stress-strain diagram, Young's modulus and Poisson's ratio of textile fibres, J. Text. March. Soc Jpn. 7 (1961) 4–12.
[38] A.M. Hartl, M. Jerabek, R.W. Lang, Anisotropy and compression/tension asymmetry of PP containing soft and hard particles and short glass fibres, eXPRESS Polym. Lett. 9 (7) (2015) 658–670.
[39] G.W. Ehrenstein, Mit Kunststoffen konstruieren. 3, Auflage, Carl Hanser Verlag, Munich, 2007.
[40] J. Kunz, Die Querkontrationszahl in der Konstruktionspraxis, KunststoffXtra, Sigwerb GmbH, Separatdruck, 2011.
[41] W. Grellmann, S. Seidler, Part 3: Mechanical and Thermomechanical Properties of Polymers: Subvolume A: Polymer Solids and Polymer Melts, Springer-Verlag, Berlin, Germany, 2014.
[42] J.E. Mark, Polymer Data Handbook, Oxford University Press, New York, 1999.
[43] E. Baur, S. Brinkmann, T.A. Osswald, E. Schmachtenberg. Saechtling Kunststoff Taschenbuch, 30. Auflage, Carl Hanser Verlag, Munich, 2007.
[44] D. Tscharnuter, M. Jerabek, Z. Major, R.W. Lang, Time-dependent poisson's ratio of polypropylene compounds for various strain histories, Mech. Time-Depend. Mater. 15 (2011) 15–28.
[45] P.h. Boulanger, M. Hayes, Poisson's ratio for orthotropic materials, J. Elast. 50 (1998) 87–89.
[46] M. Garnevičius, L. Plioplys, P.L. Ng, S. Chu, V. Gribniak, Investigation and improvement of bond performance of synthetic macro-fibres in concrete, Materials 13 (24) (2020) 5688.